Polymer-encapsulated γ-Fe2O3 nanoparticles prepared via RAFT-mediated emulsion polymerization

Keran Li, Pierre-Yves Dugas, Elodie Bourgeat-Lami, Muriel Lansalot

Polymer-encapsulated γ-Fe_2O_3 nanoparticles prepared via RAFT-mediated emulsion polymerization

Keran Li, Pierre-Yves Dugas, Elodie Bourgeat-Lami,* Muriel Lansalot*

Univ Lyon, Université Claude Bernard Lyon 1, CPE Lyon, CNRS, UMR 5265, Laboratoire de Chimie, Catalyse, Polymères et Procédés (C2P2), LCPP group, 43, Bd. du 11 Novembre 1918, F-69616 Villeurbanne, France.

ABSTRACT

Composite organic/inorganic latexes encapsulating iron oxide (IO) nanoparticles of maghemite (γ-Fe_2O_3) were successfully synthesized by surfactant-free reversible addition-fragmentation chain transfer (RAFT)-mediated emulsion polymerization. γ-Fe_2O_3 was first dispersed in an aqueous solution containing a statistical copolymer constituted of acrylic acid (AA) and *n*-butyl acrylate (BA) units, prepared by RAFT polymerization (so-called macroRAFT agent). Taking benefit from the affinity of carboxylic acid groups for iron oxide, the P(AA_{10}-*co*-BA_{10}) macroRAFT agent was adsorbed onto the surface of IO nanoparticles leading to the formation of macroRAFT/IO clusters. The interaction between the macroRAFT agent and the IO surface was investigated by the study of the adsorption isotherms, indicating that the amount of adsorbed macroRAFT agent increased with increasing macroRAFT concentration. However, a high fraction of the macroRAFT chains (up to 47%) remained in the aqueous phase. The clusters were then engaged in batch emulsion polymerization of styrene or of methyl methacrylate (MMA)/BA mixtures. IO encapsulation was however unsuccessful, and a phase separation between the polymer and the IO clusters was observed. In contrast, semi-batch emulsion polymerization of MMA/BA (90/10 wt ratio) led to effective encapsulation. Morphology studies suggest that the formation of stable latexes containing large IO clusters mainly depends on the concentration of the macroRAFT agent and the pH. Under optimized conditions, a latex with superparamagnetic properties (M_s = 16.2 emu g^{-1}) encapsulating almost all the initial IO nanoparticles was successfully produced.

Keywords: Iron oxide, RAFT, emulsion polymerization, magnetic, morphology, cryo-TEM.

1. INTRODUCTION

The synthesis of magnetic polymer particles has been focusing the attention of the scientific community for more than two decades. In most cases, these hybrid colloids incorporate magnetic iron oxide (IO) nanoparticles such as magnetite (Fe_3O_4) or maghemite (γ-Fe_2O_3), and find a wide range of applications due to their superparamagnetic properties. They can be used as solid support for purification, extraction and concentration of biomolecules in the biomedical field or for oil recovery for environmental purpose, as contrast agents in magnetic resonance imaging, as mediator in hyperthermia, or as carrier for guided drug delivery [1-6]. To efficiently play their role, these particles should meet certain criteria including an homogeneous distribution and a good encapsulation of the IO to avoid any leakage of the magnetic material, associated with a narrow particle size distribution to ensure a uniform response to an external magnetic field. Depending of the targeted utilization, the particle size must be finely tuned and appropriate surface functionalities should be considered. Particles in the submicrometer range are particularly attractive due to their low sedimentation rate and their large specific surface area for molecules immobilization.

A substantial amount of work has already been dedicated to the preparation of IO/polymer particles by free radical emulsion [7], miniemulsion [8-12], dispersion or precipitation [13] polymerization. However, to the best of our knowledge, only one of these numerous studies takes advantage of the great possibilities offered by the reversible-deactivation radical polymerization (RDRP) techniques, and more

specifically in this case, by the reversible addition-fragmentation chain transfer (RAFT) process. Indeed, Chakraborty *et al*. [14] have recently reported a RAFT-mediated miniemulsion polymerization approach involving IO nanoparticles. Using an oil soluble initiator and amphiphilic ionic liquids as surfactants, styrene polymerization was performed in the presence of an organosoluble trithiocarbonate RAFT agent carrying carboxylic acid groups, which are well-known for their affinity for the IO surface. Fine tuning of the molar ratio of the initiator and the RAFT agent and varying the final conversion led to the production of relatively stable magnetic polystyrene (PS) particles incorporating up to 27 wt% of IO (with respect to PS).

A few years ago, a surfactant-free and RAFT-based emulsion polymerization approach was proposed by Nguyen *et al*. for the direct encapsulation of inorganic particles in water [15]. The strategy employed living amphipathic random copolymers of acrylic acid (AA) and *n*-butyl acrylate (BA) adsorbed on zirconia or alumina-coated TiO_2 pigments, to encourage the emulsion polymerization to occur at the particle surface. The random nature of the copolymer prevented the macroRAFT copolymers from self-assembling into micelles, minimizing likewise the unwanted formation of new particles via micellar nucleation, while the incorporation of hydrophobic units in the polymer chains increased the affinity of the hydrophobic monomers for the particle' s environment, promoting their encapsulation. Ali *et al*. [16] confirmed the versatility of Nguyen's strategy by extending it to the encapsulation of gibbsite platelets using similar P(AA-*co*-BA) macroRAFT agents. Following the same approach, Zgheib *et al*. [17] reported the successful encapsulation

of cerium oxide (CeO_2) nanoparticles still using P(AA-*co*-BA) macroRAFT agents. The macroRAFT-mediated emulsion polymerization strategy offers a high degree of versatility with respect to the hydrophobic/hydrophilic composition and chemical nature of the macroRAFT agent, and was recently extended to the encapsulation of many kinds of inorganic particles or fillers [18-20] such as carbon nanotubes [21, 22], and silica [23]. Similar strategies were also reported for various metals (Zn, Mo), metal oxides ($BaTiO_3$, TiO_2, Al_2O_3, CuO, ZrO_2) [24], and quantum dots [25, 26], using however sodium dodecyl sulfate as molecular surfactant. To the best of our knowledge, iron oxide encapsulation has however never been reported.

In this study, IO nanoparticles were encapsulated via RAFT-mediated emulsion polymerization. As mentioned above, carboxylic acid groups can readily interact with the surface of IO. Therefore, P(AA-*co*-BA) macroRAFT agents were first synthesized before being adsorbed onto IO nanoparticles. Their adsorption induced the agglomeration of the nanoparticles, and the aggregates could not be reverted to individual particles upon sonication, leading to the formation of finite sized clusters of IO in a similar way as reported earlier by Zgheib *et al*. [17] for the encapsulation of CeO_2 nanoparticles using similar macroRAFT agents. However, compared with CeO_2, the shape of the clusters was different. The interaction between the macroRAFT agent and the IO nanoparticles was investigated by the study of adsorption isotherms, and the dispersion state of the clusters was carefully examined. The clusters were then used as seeds for the emulsion polymerization of either styrene or a monomer mixture of BA and methyl methacrylate (MMA) to form a polymeric shell around the clusters.

Both batch and semi-batch processes were evaluated, and in the latter case the impact of macroRAFT concentration, IO concentration and pH was studied.

2. EXPERIMENTAL SECTION

2.1. Materials

4,4'-azobis(4-cyanopentanoic acid) (ACPA) (Fluka, 98 %), ethyl acetate (Aldrich, anhydrous 99.8 %), acrylic acid (AA, Acros, 99.5 %), *n*-butyl acrylate (BA, 99%, Acros Organics), methyl methacrylate (MMA, 99%, Aldrich), styrene (St, 99%, Aldrich), 1,3,5-trioxane (Acros, 99.5 %) and sodium hydroxide (NaOH 0.1N, standard, Acros Organics) were used as received. Water was deionized before use (Purelab Classic UV, Elga LabWater). Iron oxide nanoparticles of maghemite (γ-Fe_2O_3) were synthesized using the coprecipitation method adapted from Massart *et al*. [27] and detailed elsewhere [28]. 4-Cyano-4-thiothiopropylsulfanyl pentanoic acid (CTPPA) was obtained by reaction of ACPA with bis(propylsulfanylthiocarbonyl) disulfide according to the literature [29].

2.2. Methods

Synthesis of the macroRAFT agent. The poly(acrylic acid-*co*-*n*-butyl acrylate) ($P(AA_{10}$-*co*-$BA_{10})$) macroRAFT agent containing a trithiocarbonate chain end was synthesized by copolymerization of AA and BA (50/50 mol%) in 1,4-dioxane at 80 °C using CTPPA as a control agent and ACPA as an initiator [17]. 0.2 mmol of

chain transfer agent (CTPPA) was introduced in a round-bottom glass flask and 0.078 mmol of 1,3,5-trioxane, 6 mmol of AA, 6 mmol of BA and 0.02 mmol of ACPA were added. The mixture was dissolved in 4 mL of 1,4-dioxane and the flask was purged with nitrogen for 30 minutes and sealed. The glass flask was then heated to 80 °C to start the polymerization. The reaction was conducted for 5h. Samples were taken during polymerization to determine conversion as a function of time and molar mass evolution with conversion. Finally, the obtained polymer was purified by precipitation in diethyl ether and characterized by size exclusion chromatography (SEC-THF) after methylation: P(AA_{10}-*co*-BA_{10}), M_n = 2040 g mol^{-1}, $Đ$ = 1.2.

Adsorption of P(AA_{10}-co-BA_{10}) macroRAFT agent onto IO nanoparticles. The adsorption of the P(AA_{10}-*co*-BA_{10}) macroRAFT agent onto IO was investigated using the depletion method as reported by Zgheib *et al*. for the adsorption of similar macroRAFT agents onto CeO_2 [17]. Briefly, different solutions of the macroRAFT copolymer (pH = 6.0) were first prepared with concentrations ranging from 4 to 20 g L^{-1}, and mixed with equal amounts of the IO dispersion (20 g L^{-1} and pH = 2.2) to cover a range of concentrations from 2 to 10 g L^{-1} (*i.e.* from 1 to 5 mmol L^{-1}) while maintaining a fixed IO concentration of 10 g L^{-1}. In each case, the macroRAFT solution was added to the IO dispersion drop by drop, which should favor the formation of large aggregates [30]. After additional stirring for 1h, the mixture was sonicated for 3 min. The purpose of sonication was to disperse the coarse aggregates formed soon after the addition of the macroRAFT agent solution. It was found that 3 min were necessary to

get clusters with the narrowest size distribution (Figure S3, Supporting Information). The dispersions were then ultracentrifuged at 80 000 rpm (Allegra^{TM} 64R Centrifuge) for 2 h to isolate the supernatant, and the macroRAFT agent concentration determined by UV analysis on the basis of a pre-established calibration curve using the specific absorption of the C=S bond of the trithiocarbonate function with a maximum at 308 nm. The adsorbed amount of macroRAFT was then calculated by difference between the initial and equilibrium concentrations according to:

$$\text{Adsorbed P(AA}_{10}\text{-}co\text{-BA}_{10}\text{) (µmol m}^{-2}\text{)} = \frac{(C_0 - C_e)V}{m} \times 100 \qquad (1)$$

where C_0 (mmol L^{-1}) is the initial macroRAFT agent concentration, C_e (mmol L^{-1}) is its equilibrium concentration in the supernatant, V (L) is the volume of solution and m (g) is the mass of iron oxide.

Emulsion polymerization in the presence of the macroRAFT agent/IO clusters. Batch emulsion polymerization reactions were performed in a 50 mL three-necked round bottom flask equipped with a condenser. As a representative example (Latex 3, Table 1), 10 mL of the cluster dispersion of IO (10 g L^{-1}) coated with P(AA_{10}-*co*-BA_{10}) (10 g L^{-1}) was placed in the flask and 0.0042 g of ACPA ([macroRAFT agent]/[ACPA] = 3) was added, followed by the addition of 1.6 g of St. This suspension was deoxygenated by purging with nitrogen for 30 min. Then, the flask was immersed in an oil bath and heated to 80 °C to start the polymerization. The same procedure was used for semi-batch experiments except for the monomer addition. 1.6 g of a deoxygenated mixture of MMA and BA (80/20, wt/wt) were fed in at a rate of 0.4 g

h^{-1} using a Dosimat autotitrator. The reaction was left 6 hours in course, 4 hours under monomer feed and 2 additional hours to complete the polymerization. Polymer conversion was determined by gravimetric analysis.

Determination of the magnetic fraction (MF) of the particles, of the IO content in the magnetic fraction (IO_{MF}) and of the fraction of magnetically-separated IO (MS_{IO}). To determine the fraction of particles that could be effectively captured by a magnet (hereafter referred to as the magnetic fraction, MF, in %), magnetic separation was applied to the final latex. Typically, a strong magnet (ferrite) was applied to the outside wall of a vial containing 1 mL of the composite latex suspension for 1 min. The magnet was then held in position and the liquid was poured out of the vial. The magnet was then removed, and the residual solid weighed after evaporation of water at 100 °C in an oven. MF was defined as:

$$MF\ (\%) = \frac{m_{\mathrm{B}}}{m_{\mathrm{A}}} \times 100 \qquad (2)$$

Where m_{A} is the total mass of solid in the latex and m_{B} is the mass of separated magnetic particles.

The IO content in the magnetic fraction (IO_{MF}, %) was then determined by thermogravimetric analyses (TGA), and used to calculate the fraction of magnetically-separated IO, MS_{IO} (%), which corresponds to the percentage of IO present in the magnetic fraction with respect to the initial amount of IO and defined as:

$$MS_{IO}\ (\%) = \frac{m_{\mathrm{IO\ separated}}}{m_{\mathrm{IO}}} \times 100 \qquad (3)$$

Where m_{IO} is the mass of IO used initially in the emulsion polymerization reaction, and $m_{IOseparated}$ is the mass of IO in the magnetic particles separated by the magnet:

$$m_{IOseparated} = \frac{IO_{MF}}{100} \times m_B \qquad (4)$$

2.3. Characterization techniques

Fourier Transform InfraRed (FTIR) spectroscopy. FTIR spectra were recorded from KBr pellets at room temperature using a Nicolet iS50 FTIR spectrometer from Thermo Scientific equipped with a deuterated triglycine sulfate (DTGS) detector. Background and sample were acquired using 32 scans at a spectral resolution of 4 cm^{-1} from 4000 to 400 cm^{-1}. Spectral data were obtained using OMNIC Software from Thermo Scientific.

^{1}H NMR spectroscopy. The individual molar conversions of AA and BA during the macroRAFT agent synthesis were determined by ^{1}H NMR spectroscopy in DMSO-d_6 at room temperature (Bruker DRX 300), by the relative integration of the protons of the internal reference (1,3,5-trioxane) and of the vinylic protons of the monomers.

Size Exclusion Chromatography (SEC). The molar masses of the macroRAFT agent were determined by Size Exclusion Chromatography in THF (THF-SEC). SEC measurements were carried out at 40 °C with a flow rate of 1 mL min^{-1} using toluene as a flow rate marker. Before analyses, carboxylic acid groups of the polymer were methylated in a THF/H_2O (90/10 v/v%) mixture using tri(methylsilyl)diazomethane as

methylation agent [31], to prevent interactions between acid groups and the stationary phase. Samples were filtered on a 0.45 μm pore size membrane and analyzed at 3 mg mL^{-1}. Separation was carried out on three columns from Malvern Instruments [T6000 M General Mixed Org (300 × 8 mm)]. The device (Viscotek TDA305) was equipped with a refractive index (RI) detector (λ = 670 nm). The number-average molar mass (M_n) and dispersity ($Đ = M_w/M_n$, with M_w: weight-average molar mass) were derived from the RI signal by a calibration curve based on polystyrene standards (PS from Polymer Laboratories).

pH measurements. pH values were measured on a Mettler Toledo SevenEasy pH meter with an InLab Routine Pro combination electrode, calibrated with 4, 7, and 10 pH buffer solutions.

Dynamic Light Scattering (DLS). The particle size (hydrodynamic diameter, D_h) was measured by DLS using the Zetasizer NanoZS instrument from Malvern. The data were collected at 173° using the fully automatic mode of the Zetasizer system, and depending on the size distribution, either the monomodal cumulant analysis or the CONTIN analysis was performed. The broadness of the distribution was given by a dimensionless number called *poly* value determined from the autocorrelation function using the second-order method of cumulant analysis.

Cryogenic-transmission electron microscopy (cryo-TEM). PMMA is known to be

particularly sensitive to electron damage. Therefore, in order to prevent degradation of the latex particles due to radiation damage at room temperature and allow reliable determination of particle morphology, all samples were characterized by cryo-TEM. The diluted samples were dropped onto 300 Mesh holey carbon films (Quantifoil R2/1) and quench-frozen in liquid ethane using a cryo-plunge workstation (made at LPS Orsay). The specimens were then mounted on a precooled Gatan 626 specimen holder, transferred in the microscope (Phillips CM120) and observed at an accelerating voltage of 120 kV (Centre Technologique des Microstructures (CTμ), platform of the Université Claude Bernard Lyon 1, Villeurbanne, France).

Magnetic measurements. A vibrating sample magnetometer (VSM, BHV-55) was used to measure the magnetization (*r*) as a function of the magnetic field intensity (*H*) at room temperature. Magnetization of both IO nanoparticles and magnetic particles was measured using the Weiss extraction method [32], decreasing the magnetic field from 21 to 0 kOe. This dynamic method makes use of the variation of flux induced in a coil when moving the sample in the field. Measurements were performed on dried samples. Specific magnetization (M in emu g^{-1}) of a given sample was defined as:

$$M = \frac{4300 \times \sigma \times \alpha}{m} \qquad (5)$$

where 4300 is the apparatus constant, m the mass of the sample (g), δ the raw electric signal value (a.u.), and α the correction of the magnetic image for strong magnetic fields. M_S, the specific saturation magnetization was obtained by extrapolation of M for strong magnetic fields ($1/H \rightarrow 0$).

Thermogravimetric analyses (TGA). The IO content in the magnetic fraction of the particles was determined by TGA on a TA instruments Q5000 IR. Typically, 10 mg of the dried sample were accurately weighed and heated from 25 to 800 °C at a rate of 10 °C min^{-1} under an oxygen atmosphere.

3. RESULTS AND DISCUSSION

The aqueous dispersion of iron oxide nanoparticles used in this study was synthesized by the precipitation of ferrous and ferric iron in an alkaline environment, followed by oxidation with $Fe(NO_3)_3$ and peptization using HNO_3 [28]. The resulting IO nanoparticles spontaneously redispersed in water to produce a colloidal sol stable at a pH around 2.2. The surface of the nanoparticles was positively charged (ζ = + 50 mV at pH = 2.2) with an isoelectric point of 7.4. The DLS analysis indicated a hydrodynamic diameter of 25 nm (*poly* = 0.25). In addition, the specific surface area determined by BET was 166 m^2 g^{-1}. These values will be used in the rest of the study.

As mentioned in the Introduction, magnetic particles should fulfill some requirements to ensure an effective magnetic separation, including the encapsulation of a high amount of IO into submicronic particles. To meet these criteria, iron oxide clusters of finite size (typically larger than 100 nm) were first prepared before being used as seeds in emulsion polymerization. To favor the formation of such clusters and then the polymerization from their surface, the adsorption of P(AA_{10}-*co*-BA_{10})

macroRAFT agents onto IO was first investigated in details.

3.1. P(AA_{10}-*co*-BA_{10}) adsorption onto IO and formation of P(AA_{10}-*co*-BA_{10}) /iron oxide clusters

The amount of P(AA_{10}-*co*-BA_{10}) adsorbed onto the IO nanoparticles was determined by the depletion method using different solutions of the macroRAFT agent mixed with equal amounts of the IO dispersion to cover copolymer concentrations ranging from 2 to 10 g L^{-1} (*i.e.* from 1 to 5 mmol L^{-1}) while maintaining a fixed IO concentration of 10 g L^{-1}. It is worth noting that the pH of the mixture was impacted by the macroRAFT concentration: the pH steadily increased from 3.2 to 4.7 when the macroRAFT concentration increased from 2 to 5 g L^{-1}, to finally level off at 6 for higher macroRAFT amounts (6 to 10 g L^{-1}). The adsorption isotherm of the P(AA_{10}-*co*-BA_{10}) macroRAFT agent onto the IO nanoparticles is shown in Figure 1a. It plots the adsorbed amount per unit area (μmol m^{-2}) as a function of the equilibrium (residual) concentration in solution, C_{eq}. The amount of adsorbed macroRAFT agent increased from 0.5 to 1.5 μmol m^{-2} with increasing the concentration of macroRAFT agent in the suspension until a plateau was reached. Indeed, the polymer chains progressively saturate the IO surface as the macroRAFT agent concentration increases. The proportion of adsorbed macroRAFT agent therefore decreased from 80% to 53% with increasing the initial macroRAFT agent concentration, indicating that an increasing part of the macroRAFT chains remained in the aqueous phase (Figure 1b).

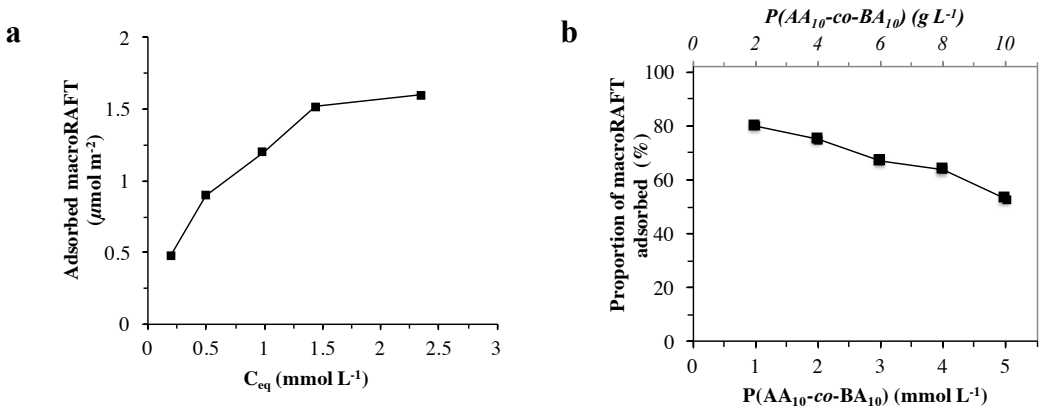

Figure 1. a) Isotherm for P(AA_{10}-*co*-BA_{10}) adsorption onto the IO surface and b) evolution of the proportion of adsorbed macroRAFT as a function of initial macroRAFT concentration. IO concentration in the final mixture: 10 g L^{-1}.

The amount of adsorbed macroRAFT was also quantified by TGA for P(AA_{10}-*co*-BA_{10}) concentrations of 1, 3 and 5 mmol L^{-1} (see Figure S1a in the Supporting Information), and the weight fraction of macroRAFT increased accordingly with the initial concentration (13, 27 and 30 wt%, respectively). The measured weight loss of the three samples was in good agreement with the amount determined by the depletion method using UV analysis (Figure S1b).

As mentioned above, macroRAFT adsorption on the IO nanoparticles led to their aggregation into finite size clusters. To gain further insight into the formation of the clusters, the size and zeta potential of the IO/macroRAFT clusters were measured as a function of the macroRAFT concentration (from 2 to 10 g L^{-1}, corresponding to 1.0 and 5.0 mmol L^{-1}) for an IO concentration in the mixture of 10 g L^{-1} (Figure 2). Again, the macroRAFT solution (pH = 6) was added to the IO dispersion and then sonicated

for 3 min. For the lowest concentrations (< 2.5 mmol L^{-1}) the IO precipitate could not be efficiently redispersed and DLS measurements were not reliable in that case as particle agglomerates could be observed by the naked eye. The size of the clusters then decreased from 1121 to 122 nm (with a *poly* value of 0.21) with increasing macroRAFT concentration from 2.5 to 5 mmol L^{-1} (Figure 2a). The observed instability at low macroRAFT concentration (≤ 2.5 mmol L^{-1}) is due to the low pH value of the suspension (from 3.2 to 4.7 as the macroRAFT concentration increases). Indeed, considering the pKa values reported for PAA ($pKa_{(PAA)}$ ≈ 6 [33]), the macroRAFT copolymer is likely protonated at low pH values, which would lead to a poor stabilization efficiency. An additional experiment was performed where the pH was increased to 6, and indeed the size of the clusters was significantly reduced (down to around 120 nm).

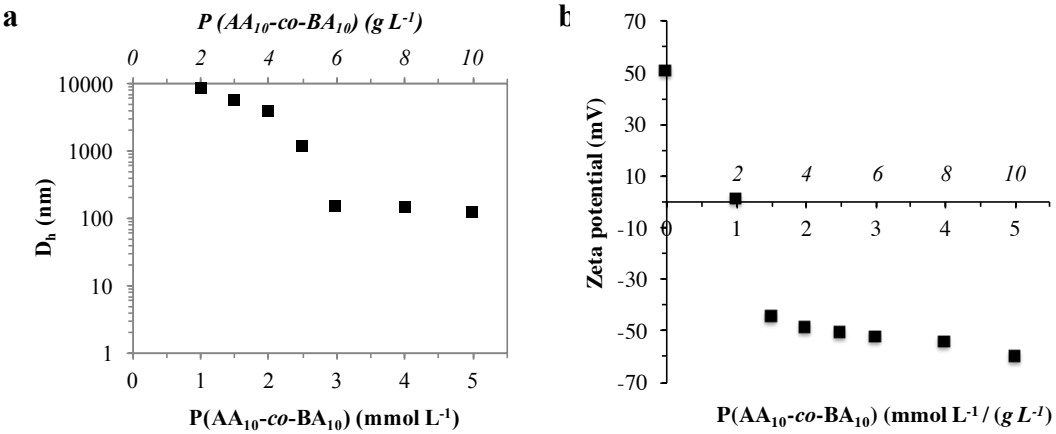

Figure 2. a) Hydrodynamic diameter and b) zeta potential of the IO/macroRAFT clusters as a function of the macroRAFT concentration. $[IO]_{mixture}$ = 10 g L^{-1}.

The zeta potential of the pristine IO nanoparticles was + 50 mV and decreased from +

0.8 mV for the lowest macroRAFT content (2 g L^{-1}, pH = 3.2) to around -60 mV for the highest macroRAFT content (10 g L^{-1}, pH = 6.0) (Figure 2b). Therefore, the stability of macroRAFT/IO clusters increased with increasing macroRAFT concentration. Zeta potential results are in agreement with the DLS results.

In addition, FTIR studies show that the macroRAFT copolymer is adsorbing through complexation between the carboxylate groups and the Fe atoms. This causes destabilization and therefore aggregation into finite sized clusters. From a more detailed investigation of the FTIR spectra (see Figure S4 and Table S1 in the Supporting Information), we hypothesize that the macroRAFT copolymer adsorbs as loops oriented flat on the surface of IO but with tails that extend into the solution in order to provide colloidal stability to the formed clusters.

Finally, the IO/macroRAFT clusters produced from the mixing of the 20 g L^{-1} IO dispersion and the 20 g L^{-1} P(AA_{10}-*co*-BA_{10}) solution (*i.e.* the point at 10 g L^{-1} or 5 mmol L^{-1} in Figure 2b) were observed by cryo-TEM (Figure 3). The clusters exhibit a non-spherical, irregular shape with a fractal geometry and a rather broad size distribution in agreement with their high *poly* values determined by DLS. A closer look at the images indicates that the clusters are slightly anisotropic with their longer dimensions roughly comprised between 70 and 130 nm, which is also in agreement with DLS (122 nm). Note that a similar fractal behavior was reported during the complexation of iron oxide nanoparticles with poly(trimethylammonium ethylacrylate)-*b*-poly (acrylamide) diblock copolymers [34, 35]. The fractal geometry of the aggregates suggests a diffusion-limited aggregation mechanism [36].

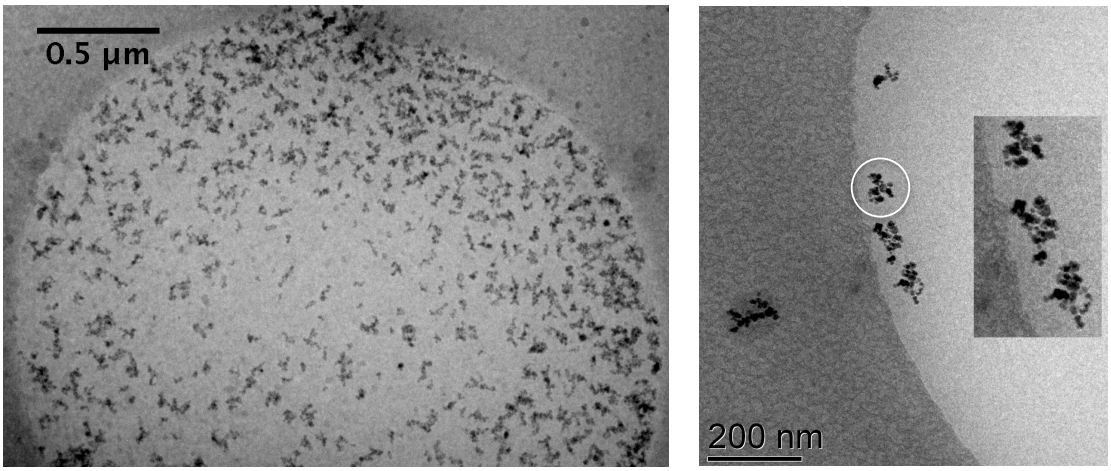

Figure 3. Cryo-TEM images of IO/macroRAFT clusters obtained when mixing the IO dispersion with the P(AA_{10}-*co*-BA_{10}) solution at pH = 6 ($[IO]_{mixture}$ = 10 g L^{-1} and $[P(AA_{10}\text{-}co\text{-}BA_{10})]_{mixture}$ = 10 g L^{-1} or 5 mmol L^{-1}). For comparison purpose, the white circle shows the size determined by DLS (D_h = 122 nm).

This first series of experiments showed that the adsorption of P(AA_{10}-*co*-BA_{10}) onto the IO nanoparticles was effective for macroRAFT concentrations comprised between 6 and 10 g L^{-1} (corresponding to a pH value of 6 for the final dispersion) leading to the formation of clusters with a size close to 120 nm, which were however not easily separated by a magnet. Therefore, many parameters were then investigated to form stable dispersions of macroRAFT/IO clusters with larger sizes: the mixing pathway (direct *versus* drop by drop), the homogenization step (time and type of device), the pH (during or after mixing), the IO concentration (10 to 60 g L^{-1}) or the macroRAFT agent concentration (10 to 40 g L^{-1}). All these methods showed that controlling at the same time the size and the dispersity of the clusters was difficult to achieve. On the one hand, stable suspensions could be obtained but with relatively small IO clusters (≤

200 nm) and reasonable dispersity (*poly* values ≤ 0.2), which could not be efficiently separated by applying an external magnetic field. On the other hand, big IO clusters could be produced (≥ 200 nm) but with large particle size distributions (*poly* values ≥ 0.3). In the range of experimental conditions studies, the formation of relatively big clusters (D_h ≥ 200 nm) with reasonable dispersities (*poly* values ≤ 0.2) was however not successful.

Consequently, the idea was to form large clusters during the emulsion polymerization step. Indeed, a partial (and limited) loss of cluster stability could result in further aggregation of IO clusters. The IO/macroRAFT clusters being more stable at pH 8 than pH 6 (information drawn from the many routes investigated to increase the cluster size), emulsion polymerizations was thus first performed at pH 6 in a batch process, using different hydrophobic monomers (either styrene or MMA/BA mixtures). The next experiments were performed in semi-batch with MMA/BA mixture (90/10 in weight). Taking into account the adsorption studies (Figure 2b), the amount of macroRAFT was gradually decreased to induce controlled cluster aggregation. On the other hand, the concentration of IO was increased to produce high IO content magnetic composite particles. The pH was also increased to 8 in some cases to improve the cluster stability. All these routes are presented in the following section.

3.2. Emulsion polymerization using macroRAFT/IO clusters as seeds

3.2.1 Batch emulsion polymerization

The first encapsulation experiments were performed in batch at pH = 6 using either a mixture of MMA and BA (90/10 wt % or 80/20 wt %) or pure styrene (Table 1). The preparation of the clusters was identical to that previously described for the adsorption studies (*i.e*. drop by drop addition of P(AA_{10}-*co*-BA_{10}) macroRAFT to the IO dispersion, followed by 1h of stirring and 3 min of sonication). P(AA_{10}-*co*-BA_{10}) and IO concentrations (both 10 g L^{-1}) were those leading to stable clusters of ca. 120 nm (Figure 2a).

Table 1. Batch emulsion polymerizations performed in the presence of P(AA_{10}-*co*-BA_{10})/IO clusters.

Latex[a]	**P(AA_{10}-*co*-BA_{10}) (g L^{-1})**	**IO (g L^{-1})**	**Monomer**	**Conv.**[c] **(%)**	$D_{h,i}/D_{h,f}$[d] **(nm)**	$poly_i/poly_f$[d]
1	10	10	MMA/BA[b] (80/20)	94	129/131	0.20/0.13
2	10	10	MMA/BA[b] (90/10)	96	123/134	0.22/0.11
3	10	10	St	92	132/161	0.21/0.23

[a] Monomer: 1.6 g / Water: 9.8 g; [macroRAFT]/[ACPA] = 3; pH = 6; reaction time = 6 h; T = 80 °C. [b] Weight ratio. [c] Final conversion determined by gravimetric analysis. [d] Initial (before monomer addition) and final diameters and *poly* values ($D_{h,i}$, $poly_i$ and $D_{h,f}$, $poly_f$ respectively) measured by DLS.

The final conversion was slightly higher for the 90/10 MMA/BA mixture (96 %) than for the 80/20 mixture (94%) or pure St (92 %). In all cases, the latex was stable with a hydrodynamic diameter close to 130 nm for the MMA/BA series, and a bit larger (D_h = 160 nm) for PSt (Table 1). It seems however that the IO particles were not encapsulated (Figure 4). Indeed, cryo-TEM images of the three latexes show the presence of aggregated clusters of IO likely located on the surface of the polymer

particles and forming a separate phase, reflecting a poor affinity between IO and the polymer phase. Moreover, the interaction between IO and the polymer particles seems lower in Latex 3 (PSt) than in Latex 1 or 2. This is likely because St is more hydrophobic than MMA and BA. Therefore, St has a poorer affinity for the macroRAFT-coated IO particles than MMA or BA, and so do the resulting polymers. In addition, a population of pure polymer particles can also be clearly identified on the micrographs. The presence of this population of secondary nucleated particles may be related to the amount of free macroRAFT in water. Indeed, the adsorption isotherm in Figure 1b shows that only 53 % of the macroRAFT agent is adsorbed on the IO surface under the conditions used in the emulsion polymerizations (*i.e.* [IO] = [macroRAFT] = 10 g L^{-1}, Table 1), while the remaining 47 % stays in the aqueous phase. As a result, chain extension of these free P(AA_{10}-*co*-BA_{10}) chains in water with BA/MMA or St leads to amphiphilic block copolymers which are able to self-assemble to form polymer particles devoid of IO according to the polymerization-induced self-assembly process [19, 37, 38]. Several hypotheses can be put forward to explain the failure of IO encapsulation. First, the presence of monomer droplets may promote macroRAFT desorption from the IO surface. The adsorbed amount would be then lower than the minimum amount necessary for successful encapsulation. This may be accentuated by the formation of the secondary nucleated particles, which may also compete for macroRAFT adsorption to the detriment of encapsulation. Second, the monomer accumulated in the polymer particles may act as a plasticizing agent, increasing polymer chain mobility and allowing the IO clusters to

migrate to the polymer/water interface in a thermodynamically controlled process. Note that a similar phase separation phenomenon was already reported in the literature using a related macroRAFT strategy in batch [17, 21, 23].

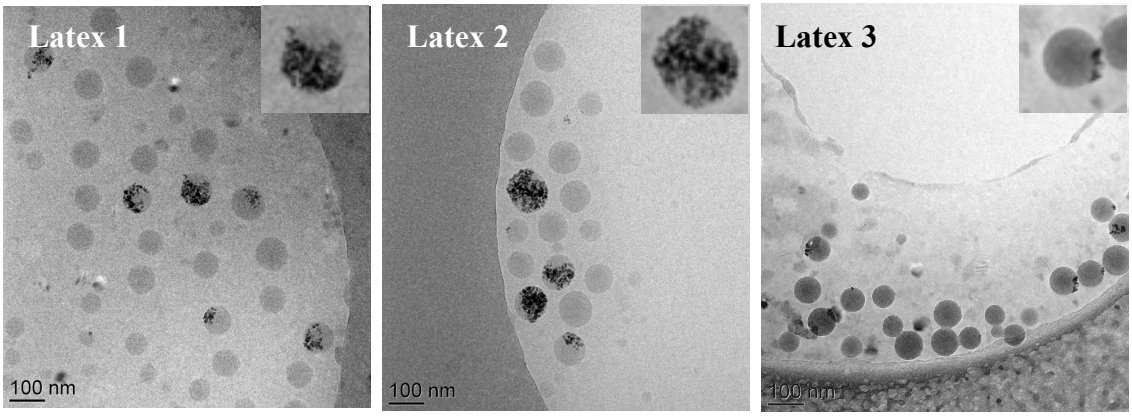

Figure 4. Cryo-TEM images of the latex particles obtained after batch emulsion polymerization of hydrophobic monomer(s) in the presence of IO clusters (10 g L^{-1}) coated with P(AA_{10}-*co*-BA_{10}) macroRAFT agent (10 g L^{-1}). Latex 1: MMA/BA 80/20 (wt/wt), Latex 2: MMA/BA 90/10 (wt/wt) and Latex 3: pure St. The inset shows a magnified portion of the image.

3.2.2 Semi-batch emulsion polymerization

The previous results showed the limits of the batch process to ensure IO encapsulation. Therefore, the next series of experiments were performed in semi-batch. Indeed, the process used for the encapsulation of inorganic particles in the presence of macroRAFT agents, either batch or semi-batch, has been shown to influence the overall mechanism of encapsulation [18-20]. As mentioned in the previous section, monomer droplets are present in a batch process and the macroRAFT agents may thus partition between the different phases. In addition, the monomer may act as a plasticizer, decreasing the glass transition temperature of the copolymer shell,

promoting polymer chain mobility, which may push the inorganic particles towards the polymer/water interface. All or part of these drawbacks should be avoided, at least minimized, in a semi-batch process.

The detailed experimental procedure is presented in the experimental section. The protocol followed for the formation of the macroRAFT/IO clusters was the same as for the batch process, except that after stirring for 1h, the clusters were prepared either by sonication (when the pH was 6) or by sonication followed by a pH increase to 8. The encapsulation experiments were in all cases performed with a semi-continuous feed of MMA/BA (90/10 wt/wt) (Table 2).

Table 2. Semi-batch emulsion polymerizations of MMA/BA (90/10 in weight) performed in the presence of IO coated with P(AA_{10}-*co*-BA_{10}).

Latex[a]	**IO** (g L^{-1})	**macroRAFT** (g L^{-1})	**pH**[b]	**Conv.**[c] (%)	$D_{h,i}/D_{h,f}$[d] (nm)	$poly_i/poly_f$[d]	**MF**[e] (%)	IO_{MF}[f] (%)	MS_{IO}[g] (%)
4	10	10	6	81	121/125	0.20/0.17	13	19	35
5	10	8	6	82	132/151	0.21/0.12	18	18	44
6	10	6	6	77	146/157	0.17/0.12	36	15	75
7	20	20	6	87	135/137	0.20/0.17	23	20	36
8	30	30	6	86	135/142	0.20/0.21	33	21	38
9	40	40	6	89	139/146	0.17/0.16	44	20	40
10	40	30	6	86	140/149	0.17/0.15	62	22	62
11	40	25	6	85	142/152	0.19/0.16	85	25	95
12	40	20	6	Unstable clusters					
13	40	20	8	76	91/135	0.19/0.19	72	24	73
14	40	10	8	71	94/178	0.17/0.21	95	28	99
15	40	8	8	/	102/unstable	0.20/unstable			

[a] Water: 9.8 g; Monomer: 1.6 g (feed rate = 0.4 g h^{-1}); [macroRAFT]/[ACPA] = 3; reaction time = 6.0 h; T = 80 °C. [b] pH of IO/macroRAFT mixture. [c] Final conversion determined by gravimetric analysis. [d] Initial (before monomer addition) and final diameters and poly values ($D_{h,i}$, $poly_i$ and $D_{h,f}$, $poly_f$ respectively) measured by DLS. [e] Magnetic fraction of the particles determined using equation (2). [f] IO content of the magnetic fraction as determined by TGA. [g] Fraction of magnetically-separated IO calculated using equation (3).

In the first series of experiments (Latex 4, 5 and 6), the IO concentration was kept at 10 g L^{-1}, while the concentration of macroRAFT agent was decreased from 10 to 6 g L^{-1}. These concentrations correspond to the conditions used in the adsorption experiments shown in Figure 2, leading to a pH value of 6 for the IO/macroRAFT dispersion. As expected, the IO cluster size showed a slight increase from 121 nm to 146 nm with a decrease of macroRAFT agent concentration from 10 to 6 g L^{-1}. The latexes obtained after emulsion polymerization were stable. For the three experiments, DLS results showed a slight increase in the particle size, which could be consistent with a successful encapsulation of the starting clusters. Indeed, the corresponding cryo-TEM images (Figure 5) confirmed that IO was exclusively located in the latex particles, with however an uneven distribution among the loaded particles probably correlated with the rather broad distribution in size of the initial clusters. Cryo-TEM also shows a good agreement with the DLS results. Yet, many free latex particles and small magnetic composites were observed in the three samples. Interestingly, the composite particles have an irregular shape that may follow the shape of the original IO nanoclusters, which suggests that the clusters have been acting as seeds for the emulsion polymerization. When the macroRAFT concentration decreased (from Latex 4 to 6), the fraction of pure polymer particles decreased. Indeed, the proportion of free macroRAFT (determined from the adsorption isotherm in Figure 1b) was 47% in Latex 4, which was higher than for Latex 5 (36%) and Latex 6 (33%) and, as mentioned above, the presence of free macroRAFT promotes secondary nucleation. Because the total amount of monomer was kept the same (1.6 g) in all the experiments,

the thickness of the polymer shell logically increased when the fraction of secondary-nucleated particles decreased.

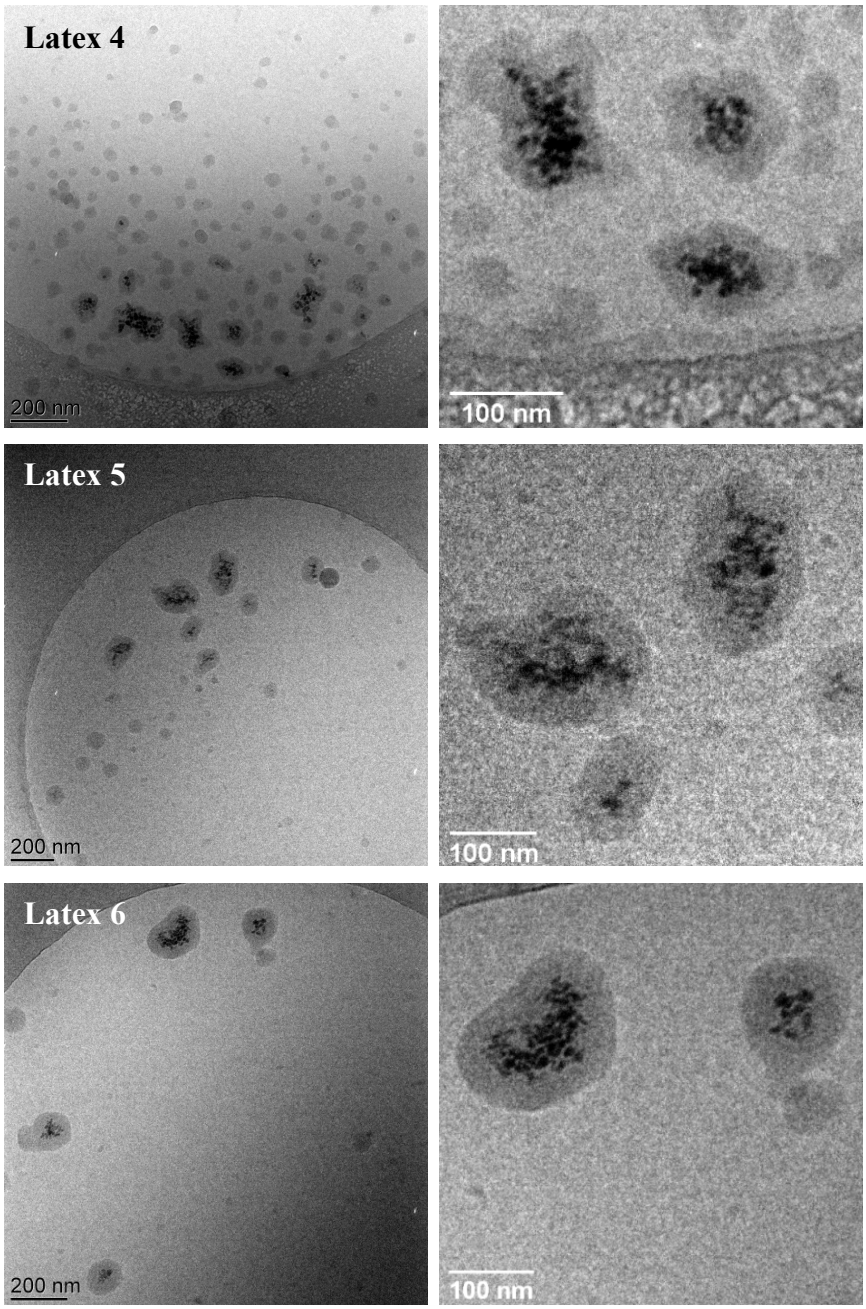

Figure 5. Left: cryo-TEM images of the polymer-IO composite particles obtained after emulsion polymerization of MMA/BA (90/10) in the presence of IO clusters coated with P(AA_{10}-*co*-BA_{10}) macroRAFT agent (pH = 6) prepared using various concentrations of macroRAFT (Latex 4 to 6, See Table 2 for detailed experimental conditions). Right: same samples at higher magnification.

The fraction of separated magnetic particles (MF), the IO amount in the magnetic fraction (IO_{MF}) and the fraction of magnetically-separated IO (MS_{IO}) were then determined to confirm TEM observations. The MF increased from 13% to 36% with decreasing the macroRAFT concentration. In other words, the fraction of the pure polymer particles and of the composite ones that were not magnetic enough to be separated by the magnet decreased. In addition, TGA showed that the IO content in the magnetic fraction, IO_{MF}, decreased from 19% to 15%, which was in agreement with the increase of shell thickness. Nevertheless, as mentioned above, the magnetic fraction, MF, increased when the macroRAFT concentration decreased, indicating that more IO nanoparticles were encapsulated, or at least present in aggregates big enough to allow their magnetic separation. Accordingly, MS_{IO} increased from 35 % to 75 % with decreasing macroRAFT concentration from 10 to 6 g L^{-1}.

In order to further increase the amount of IO in the final latex, the concentration of both IO and P(AA_{10}-*co*-BA_{10}) was increased to 20 g L^{-1}, 30 g L^{-1} and 40 g L^{-1} (Latex 7, 8 and 9). The IO cluster size of the three samples before polymerization was almost the same, around 135 nm (in accordance with the results of the preliminary experiments, data not shown). This series of latexes showed results similar to those obtained for lower IO and macroRAFT contents (Latex 4, 10 g L^{-1} of both IO and macroRAFT). Indeed, secondary nucleation occurred due to the presence of free macroRAFT as could be expected from the previous adsorption studies (Figure 1b), as ca. 50% of the macroRAFT should remain in water. Again, the particles showed

distorted shapes, which may be similar to those of the original clusters. The IO particles were not uniformly distributed among the composite particles, which could be related to the size inhomogeneity of the original clusters (Figure 6). Indeed, some contained a lot of IO while others contained only one or two IO nanoparticles. In this group of experiments, MF increased from 23% to 44% in good agreement with the increase of the initial IO content (from 20 to 40 g L^{-1}). IO_{MF} was nevertheless similar for the 3 latexes (ca. 20%), and so was MS_{IO} (38 ± 2%). The distribution of IO inside the polymer particles looked similar in the three cases.

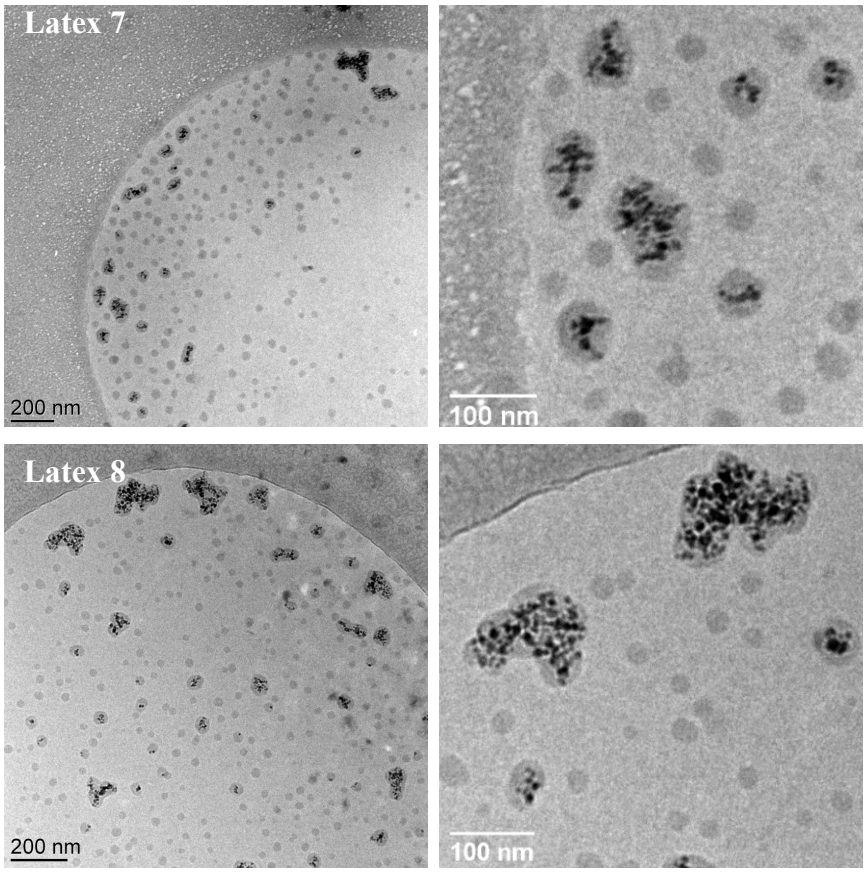

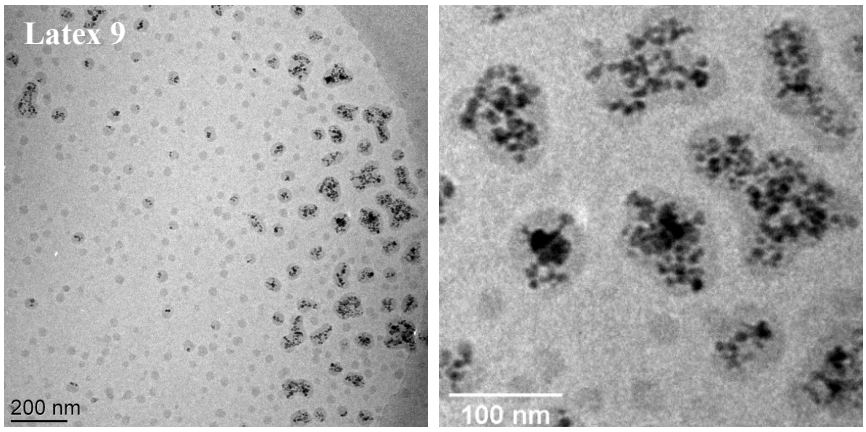

Figure 6. Left: cryo-TEM images of the polymer-IO composite particles obtained after emulsion polymerization of MMA/BA (90/10 in weight) in the presence of IO clusters coated with P(AA_{10}-*co*-BA_{10}) macroRAFT agent prepared using varying IO and macroRAFT concentrations (pH = 6) for a fixed 1:1 ratio (Latex 7 to 9, Table 2). Right: same samples at higher magnification.

To decrease the secondary nucleation while keeping the uniformity of IO clusters, the concentration of macroRAFT agent was first decreased to 30 and 25 g L^{-1} (Latex 10 and 11, respectively) keeping a constant IO concentration of 40 g L^{-1}. The size of the clusters only slightly increased compared to Latex 9 (140 and 142 nm *versus* 139 nm). Accordingly, the size of the final particles slightly increased from 146 to 152 nm (Latex 9, 10 and 11 in Table 2). Cryo-TEM images clearly show that the amount of free particles decreases gradually with decreasing the concentration of macroRAFT agent (Figures 6 and 7).

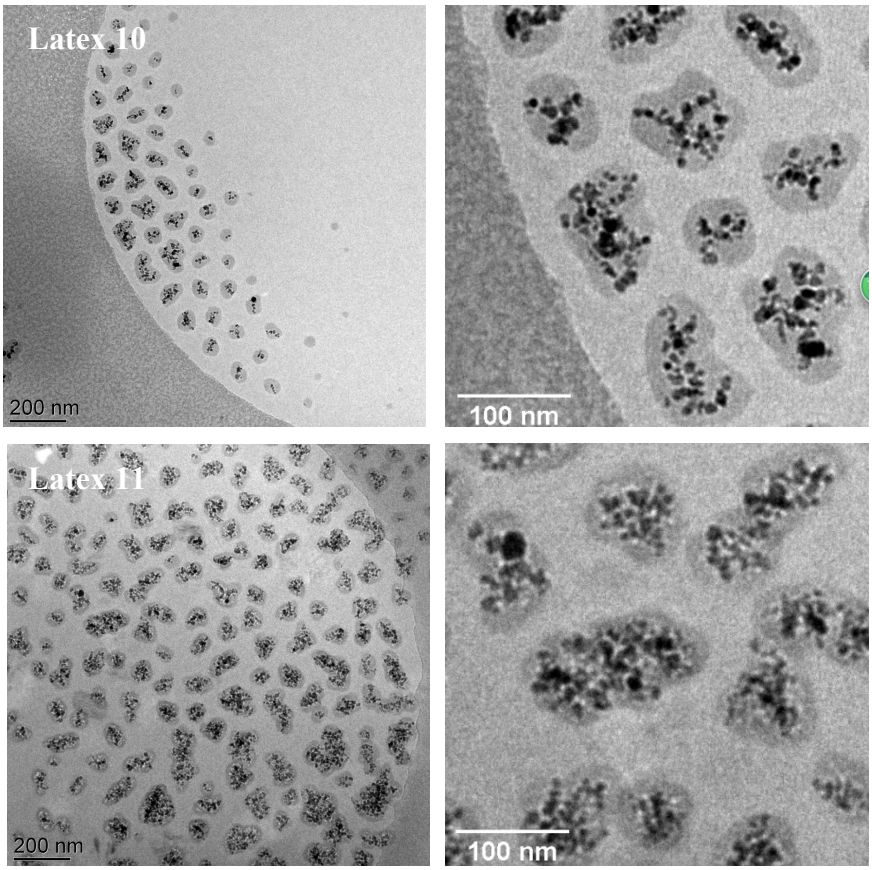

Figure 7. Left : cryo-TEM images of the polymer-IO composite particles obtained after emulsion polymerization of MMA/BA (90/10) in the presence of IO clusters coated with P(AA_{10}-*co*-BA_{10}) macroRAFT agent (pH = 6) prepared using various concentrations of macroRAFT (Latex 10 and 11, See Table 2 for detailed experimental conditions). Right: same samples at higher magnification.

Accordingly, MF increased from 44% to 85%, accompanied by a slight increase of IO_{MF} (20 to 25%). TGA confirmed that MS_{IO} also increased from 40% to 95%. In order to increase the size of the IO clusters and consequently that of the final composite particles, the concentration of macroRAFT agent was further decreased to 20 g L^{-1} (Latex 12). However, the clusters were not stable. It seems that a minimal amount of macroRAFT (for a given concentration of IO) is necessary to maintain the

stability. This is in agreement with the DLS results shown in Figure 2a. Nevertheless, decreasing the concentration of macroRAFT agent, within a certain range, allows the synthesis of bigger magnetic composite particles.

As the use of less macroRAFT agent clearly impacts the stability of the final latex, the influence of the initial IO/macroRAFT cluster stability was then investigated by varying the pH of the IO/macroRAFT mixture. Indeed, right after the preparation of the clusters, the pH was raised to 8. Whereas no stable clusters were obtained for Latex 12, for the same concentration of both IO and macroRAFT, the additional step of pH increase allowed the formation of stable clusters (Latex 13, Table 2), with a diameter of 91 nm. This improvement can reasonably be associated with the contribution of more carboxylate groups to the stability of the clusters. After polymerization, Latex 13 was stable with a diameter of 135 nm, higher than that of the clusters, which clearly indicates partial aggregation during the polymerization. The pH increase from 6 to 8 was thus able to provide stable clusters but the amount of macroRAFT was however likely not high enough to provide stability to the growing particles. Some particles thus aggregated to reduce the total surface area. This experiment thus indicates that the stability of the latex depends on both the concentration of the macroRAFT agent and the pH. Cryo-TEM image of this latex showed that encapsulated particles were smaller than those from Latex 11 for instance, and that many particles only incorporated a few IO nanoparticles (Figure 8). Therefore, some composite particles (with low IO amount) could not be separated magnetically. The fraction of separated magnetic particles was 72% with still a IO_{MF}

value close to 25 %. The fraction of magnetically-separated IO, MS_{IO}, was 73 %.

In order to produce larger particles, the concentration of macroRAFT agent was decreased to 10 g L^{-1} (Latex 14). The size of this stable latex (178 nm) was almost twice as much as that of the initial IO cluster (94 nm). Again, this clearly indicates that the IO clusters partially aggregated during the polymerization. Cryo-TEM image of the latex also confirmed the presence of larger magnetic composite nanoparticles (Figure 8). 95 % of the latex particles could be separated magnetically, with a IO_{MF} value of 28%, and MS_{IO} reaching 99%. Nevertheless, when the concentration of macroRAFT agent was further decreased to 8 g L^{-1} (Latex 15), the macroRAFT agent was not able to maintain the stability of the particles during the polymerization, even if the clusters were stable at the beginning (102 nm).

The three last experiments (*i.e.* Latex 13 to 15) clearly show the crucial role played by the initial concentration of the macroRAFT agent, which should ensure a good balance between the amount of macroRAFT adsorbed onto the IO clusters and the amount of free polymer chains present in the continuous phase. Indeed, as previously mentioned in the literature[15] it appears that a certain quantity of free macroRAFT is necessary to maintain the stability of the growing particles while their surface area increases during the polymerization. However, this concentration should remain low enough to prevent secondary nucleation. Based on the adsorption isotherm presented in Figure 1, the concentration of free macroRAFT decreases from Latex 13 to Latex 15, where this concentration is actually too low to ensure the stability.

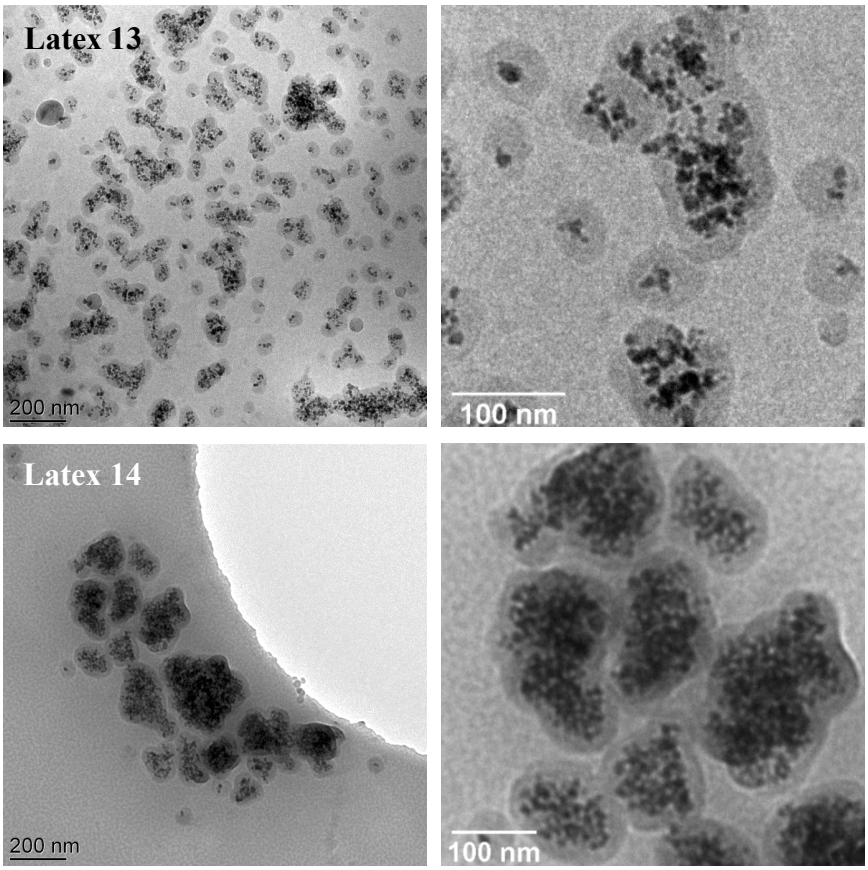

Figure 8. Left : cryo-TEM images of the polymer-IO composite particles obtained after emulsion polymerization of MMA/BA (90/10) in the presence of IO clusters coated with P(AA_{10}-*co*-BA_{10}) macroRAFT agent (pH = 8) prepared using various concentrations of macroRAFT (Latex 13 and 14, See Table 2 for detailed experimental conditions). Right : same samples at higher magnification.

Finally, the magnetic properties of the latex exhibiting the most promising features, *i.e.* Latex 14 (Table 2), were investigated. When a magnet was applied for 1 min, almost all the magnetic composite nanoparticles could be separated (MF = 95 %). The magnetic properties of the separated composite nanoparticles from Latex 14 were then investigated using a vibrating sample magnetometer. Figure 9 shows the magnetization curve of the latex. The magnetic particles possess superparamagnetic properties as no remanence was observed when the magnetic field was removed. The

saturation magnetization M_s was 16.2 emu g^{-1}. A comparison with bulk IO indicates that the amount of IO in this latex was 27 wt %, which was in good agreement with the TGA data, 28 wt % (Figure S2 in the Supporting Information).

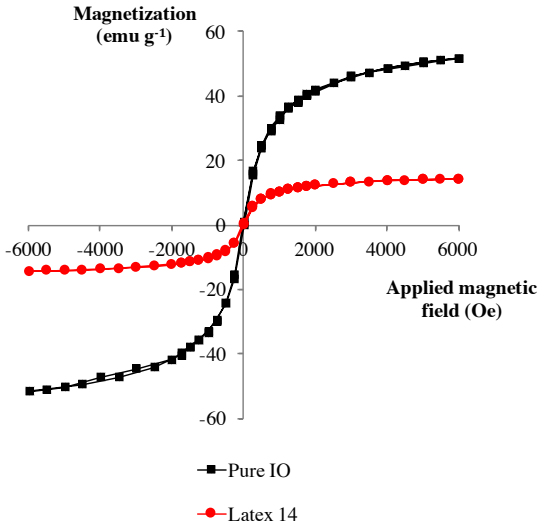

Figure 9. Magnetization versus applied magnetic field curve of the magnetic fraction of Latex 14 recovered after exposing the hybrid suspension to a magnet for 1 min. The magnetization is given per gram of composite particles.

CONCLUSIONS

Composite organic/inorganic latexes encapsulating IO nanoparticles were successfully synthesized by surfactant-free RAFT-mediated emulsion polymerization using P(AA_{10}-*co*-BA_{10}) macroRAFT copolymers to both stabilize the initial iron oxide dispersion and to facilitate the growth of polymer onto the inorganic surface. Taking benefit from the affinity of carboxylic acid groups for transition metal oxides, P(AA_{10}-*co*-BA_{10}) macroRAFT copolymers carrying a trithiocarbonate chain end were adsorbed onto the surface of IO leading to the formation of macroRAFT/IO clusters. From the adsorption isotherm, the mass of macroRAFT agent adsorbed on the IO

surface increased with increasing macroRAFT concentration. However, a high amount of the macroRAFT chains (up to 47%) remained in the aqueous phase. Batch emulsion polymerization of St or of MMA/BA mixtures resulted in unsuccessful encapsulation, leading to a phase separation between the polymer and the IO cluster. During batch emulsion polymerization, the polymer chains grew not only on the IO clusters surface but also in water. In contrast, semi-batch emulsion polymerization of MMA/BA (90/10 wt ratio) led to effective encapsulation, the polymer shell following the irregular contours of the original clusters. Morphology studies suggest that the formation of stable latexes containing large IO clusters mainly depends on the pH and the concentration of the macroRAFT agent. The concentration of the latter must be high enough to ensure the cluster formation and their stability, while providing free macroRAFT agents in the continuous phase that will participate to the stabilization of the growing composite particles. In addition, we showed that working at pH 8 rather than 6 allowed reducing the amount of macroRAFT agent while forming smaller clusters that however underwent partial aggregation during the polymerization, which *in fine* led to bigger particles. In the best case, a stable latex (178 nm) encapsulating almost all the initial IO nanoparticles (99%) with 95% of the particles being magnetic was produced. This composite latex exhibited superparamagnetic properties (M_s = 16.2 emu g^{-1}).

ACKNOWLEDGMENTS

Financial support from the Chinese Scholarship Council is gratefully acknowledged.

REFERENCES

[1] A.-H. Lu, E. L. Salabas and F. Schüth, Magnetic Nanoparticles: Synthesis, Protection, Functionalization, and Application, Angew. Chem. Int. Ed. 46 (2007) 1222-1244.

[2] U. Jeong, X. Teng, Y. Wang, H. Yang and Y. Xia, Superparamagnetic Colloids: Controlled Synthesis and Niche Applications, Adv. Mater. 19 (2007) 33-60.

[3] C. Boyer, M. R. Whittaker, V. Bulmus, J. Liu and T. P. Davis, The design and utility of polymer-stabilized iron-oxide nanoparticles for nanomedicine applications, NPG Asia Mater. 2 (2010) 23-30.

[4] O. Philippova, A. Barabanova, V. Molchanov and A. Khokhlov, Magnetic polymer beads: Recent trends and developments in synthetic design and applications, Eur. Polym. J. 47 (2011) 542-559.

[5] A. Pavía-Sanders, S. Zhang, J. A. Flores, J. E. Sanders, J. E. Raymond and K. L. Wooley, Robust Magnetic/Polymer Hybrid Nanoparticles Designed for Crude Oil Entrapment and Recovery in Aqueous Environments, ACS Nano 7 (2013) 7552-7561.

[6] S. Kalia, S. Kango, A. Kumar, Y. Haldorai, B. Kumari and R. Kumar, Magnetic polymer nanocomposites for environmental and biomedical applications, Colloid Polym. Sci. 292 (2014) 2025-2052.

[7] E. Bourgeat-Lami and M. Lansalot, Organic/Inorganic Composite Latexes: The Marriage of Emulsion Polymerization and Inorganic Chemistry, Adv. Polym. Sci. 233 (2010) 53-123.

[8] J. Hu, M. Chen and L. Wu, Organic-inorganic nanocomposites synthesized via miniemulsion polymerization, Polym. Chem. 2 (2011) 760-772.

[9] C. Weiss and K. Landfester, Miniemulsion Polymerization as a Means to Encapsulate Organic and Inorganic Materials, Adv. Polym. Sci. 233 (2010) 185-236.

[10] D. Qi, Z. Cao and U. Ziener, Recent advances in the preparation of hybrid nanoparticles in miniemulsions, Adv. Colloid Interface Sci. 211 (2014) 47-62.

[11] J. M. Asua, Challenges for Industrialization of Miniemulsion Polymerization, Prog. Polym. Sci. 39 (2014) 1797–1826.

[12] C. Flesch, Y. Unterfinger, E. Bourgeat-Lami, E. Duguet, C. Delaite and P. Dumas, Poly(ethylene glycol) surface coated magnetic particles, Macromolecular Rapid Communications 26(18) (2005) 1494-1498.

[13] M. Rahman and A. Elaissari, Organic–Inorganic Hybrid Magnetic Latex, Adv. Polym. Sci. 233 (2010) 237-281.

[14] S. Chakraborty, K. Jähnichen, H. Komber, A. A. Basfar and B. Voit, Synthesis of Magnetic Polystyrene Nanoparticles Using Amphiphilic Ionic Liquid Stabilized RAFT Mediated Miniemulsion Polymerization, Macromolecules 47 (2014) 4186-4198.

[15] D. Nguyen, H. S. Zondanos, J. M. Farrugia, A. K. Serelis, C. H. Such and B. S. Hawkett, Pigment Encapsulation by Emulsion Polymerization Using Macro-RAFT Copolymers, Langmuir 24 (2008) 2140-2150.

[16] S. I. Ali, J. P. A. Heuts, B. S. Hawkett and A. M. van Herk, Polymer Encapsulated Gibbsite Nanoparticles: Efficient Preparation of Anisotropic Composite Latex Particles by RAFT-Based Starved Feed Emulsion Polymerization, Langmuir 25 (2009) 10523-10533.
[17] N. Zgheib, J.-L. Putaux, A. Thill, E. Bourgeat-Lami, F. D'Agosto and M. Lansalot, Cerium oxide encapsulation by emulsion polymerization using hydrophilic macroRAFT agents, Polymer Chemistry 4 (2013) 607-614.
[18] A. Cenacchi-Pereira, E. Grant, F. D'Agosto, M. Lansalot and E. Bourgeat-Lami, Encapsulation with the Use of Controlled Radical Polymerization, in: S. Kobayashi and K. Müllen (Eds.), Encyclopedia of Polymeric Nanomaterials Springer Berlin Heidelberg 2014, pp. 1-13.
[19] P. B. Zetterlund, S. C. Thickett, S. Perrier, E. Bourgeat-Lami and M. Lansalot, Controlled/Living Radical Polymerization in Dispersed Systems: An Update, Chemical Reviews 115 (2015) 9745–9800.
[20] E. Bourgeat-Lami, F. D'Agosto and M. Lansalot, Synthesis of Nanocapsules and Polymer/Inorganic Nanoparticles Through Controlled Radical Polymerization At and Near Interfaces in Heterogeneous Media, Adv. Polym. Sci. 270 (2016) 123-161.
[21] W. Zhong, J. N. Zeuna and J. P. Claverie, A versatile encapsulation method of noncovalently modified carbon nanotubes by RAFT polymerization, Journal of Polymer Science Part A: Polymer Chemistry 50 (2012) 4403-4407.
[22] D. Nguyen, C. H. Such and B. S. Hawkett, Polymer coating of carboxylic acid functionalized multiwalled carbon nanotubes via reversible addition-fragmentation chain transfer mediated emulsion polymerization, J. Polym. Sci. Part A: Polym. Chem. 51 (2013) 250-257.
[23] E. Bourgeat-Lami, A. J. Palmeira Galvao de França, T. de Camargo Chaparro, R. Duarte Silva, P.-Y. Dugas, G. Alves and A. Martins Dos Santos, Synthesis of polymer/silica hybrid latexes by surfactant-free RAFT-mediated emulsion polymerization Macromolecules DOI: 10.1021/acs.macromol.6b00737 (2016).
[24] J.-C. Daigle and J. P. Claverie, A Simple Method for Forming Hybrid Core-Shell Nanoparticles Suspended in Water, J. Nanomater. 2008 (2008) Article ID 609184.
[25] P. Das, W. Zhong and J. Claverie, Copolymer nanosphere encapsulated CdS quantum dots prepared by RAFT copolymerization: synthesis, characterization and mechanism of formation, Colloid Polym. Sci. 289 (2011) 1519-1533.
[26] P. Das and J. P. Claverie, Synthesis of single-core and multiple-core core-shell nanoparticles by RAFT emulsion polymerization: Lead sulfide-copolymer nanocomposites, J. Polym. Sci. Part A: Polym. Chem. 50 (2012) 2802-2808.
[27] R. Massart, Preparation of Aqueous Magnetic Liquids in Alkaline and Acidic Media, IEEE Trans. Magn. 17 (1981) 1247-1248.
[28] K. Li, P.-Y. Dugas, M. Lansalot and E. Bourgeat-Lami, Surfactant-free emulsion polymerization stabilized by ultrasmall superparamagnetic iron oxide particles using acrylic acid or methacrylic acid as auxiliary comonomers, Macromolecules (2016) Submitted.
[29] T. Boursier, I. Chaduc, J. Rieger, F. D'Agosto, M. Lansalot and B. Charleux, Controlled radical polymerization of styrene in miniemulsion mediated by PEO-based

trithiocarbonate macromolecular RAFT agents, Polym. Chem. 2 (2011) 355-362.
[30] L. Qi, J. Fresnais, J.-F. Berret, J.-C. Castaing, I. Grillo and J.-P. Chapel, Influence of the Formulation Process in Electrostatic Assembly of Nanoparticles and Macromolecules in Aqueous Solution: The Mixing Pathway, J. Phys. Chem. C 114 (2010) 12870-12877.
[31] N. Hashimoto, T. Aoyama and T. Shioiri, New Methods and Reagents in Organic Synthesis. A Simple Efficient Preparation of Methyl Esters with Trimethylsilyldiazomethane (TMSCHN2) and Its Application to Gas Chromatographic Analysis of Fatty Acids, Chemical and Pharmaceutical Bulletin 29 (1981) 1475-1478.
[32] N. Joumaa, P. Toussay, M. Lansalot and A. Elaissari, Surface modification of iron oxide nanoparticles by a phosphate-based macromonomer and further encapsulation into submicrometer polystyrene particles by miniemulsion polymerization, J. Polym. Sci. Part A: Polym. Chem. 46 (2008) 327-340.
[33] F. A. Plamper, H. Becker, M. Lanzendörfer, M. Patel, A. Wittemann, M. Ballauff and A. H. E. Müller, Synthesis, Characterization and Behavior in Aqueous Solution of Star-Shaped Poly(acrylic acid), Macromol. Chem. Phys. 206 (2005) 1813-1825.
[34] J.-F. Berret, N. Schonbeck, F. Gazeau, D. El Kharrat, O. Sandre, A. Vacher and M. Airiau, Controlled Clustering of Superparamagnetic Nanoparticles Using Block Copolymers: Design of New Contrast Agents for Magnetic Resonance Imaging, J. Am. Chem. Soc. 128 (2006) 1755-1761.
[35] J.-F. Berret, A. Sehgal, M. Morvan, O. Sandre, A. Vacher and M. Airiau, Stable oxide nanoparticle clusters obtained by complexation, J. Colloid Interface Sci. 303 (2006) 315-318.
[36] M. Y. Lin, H. M. Lindsay, D. A. Weitz, R. C. Ball, R. Klein and P. Meakin, Universality in colloid aggregation, Nature 339 (1989) 360-362.
[37] S. L. Canning, G. N. Smith and S. P. Armes, A Critical Appraisal of RAFT-Mediated Polymerization-Induced Self-Assembly, Macromolecules 49 (2016) 1985-2001.
[38] M. Lansalot, J. Rieger and F. D'Agosto, Polymerization-Induced Self-Assembly: the Contribution of Controlled Radical Polymerization to the Formation of Self-Stabilized Polymer Particles of Various Morphologies, in: O. Borisov and L. Billon (Eds.), Macromolecular self-assembly 2016.